ELSEVIER

RESEARCH: Short Communication

3D printing metals like thermoplastics: Fused filament fabrication of metallic glasses

Michael A. Gibson [1,2], Nicholas M. Mykulowycz [1], Joseph Shim [1], Richard Fontana [1], Peter Schmitt [1], Andrew Roberts [1], Jittisa Ketkaew [4] Ling Shao [4], Wen Chen [5], Punnathat Bordeenithikasem [4], Jonah S. Myerberg [1], Ric Fulop [1], Matthew D. Verminski [1], Emanuel M. Sachs [1,3], Yet-Ming Chiang [1,2], Christopher A. Schuh [1,2], A. John Hart [1,3], Jan Schroers [1,4,*]

[1] Desktop Metal, Inc., Burlington, MA 01803, United States
[2] Department of Materials Science and Engineering, Massachusetts Institute of Technology, Cambridge, MA 02139, United States
[3] Department of Mechanical Engineering, Massachusetts Institute of Technology, Cambridge, MA 02139, United States
[4] Department of Mechanical Engineering & Materials Science, Yale University, New Haven, CT 06520, United States
[5] Department of Mechanical and Industrial Engineering, University of Massachusetts, Amherst, MA 01003, United States

Whereas 3D printing of thermoplastics is highly advanced and can readily create complex geometries, 3D printing of metals is still challenging and limited. The origin of this asymmetry in technological maturity is the continuous softening of thermoplastics with temperature into a readily formable state, which is absent in conventional metals. Unlike conventional metals, bulk metallic glasses (BMGs) demonstrate a supercooled liquid region and continuous softening upon heating, analogous to thermoplastics. Here we demonstrate that, in extension of this analogy, BMGs are also amenable to extrusion-based 3D printing through fused filament fabrication (FFF). When utilizing the BMGs' supercooled liquid behavior, 3D printing can be realized under similar conditions to those in thermoplastics. Fully dense and amorphous BMG parts are 3D printed in ambient environmental conditions resulting in high-strength metal parts. Due to the similarity between FFF of thermoplastics and BMGs, this method may leverage the technology infrastructure built by the thermoplastic FFF community to rapidly realize and proliferate accessible and practical printing of metals.

Introduction

The materials toolbox has traditionally demanded hard choices [1]. While the structural performance of metals is superior to that of thermoplastics, processing of metals is generally challenging (Fig. 1). In contrast, plastics, particularly thermoplastics, can be readily processed into complex geometries, but exhibit inferior structural performance [1]. The high processability of thermoplastics originates from their continuous softening with temperature into a readily formable state.

In principle, two strategies allow to escape this property-processing trade off. One strategy is the development of novel processing methods which are outside conventional processing strategies. A contemporary example is additive manufacturing (AM), which, for thermoplastics, has enabled 3D printing of complex shapes through a material extrusion process, called fused filament fabrication (FFF). In contrast, the versatility and practicality for AM of metals lags significantly behind [2]. This is essentially due to the inability to maintain metals at viscosities on practical time scales that would be suited for processing/forming operations such as material extrusion in FFF processes (Fig. 1)

* Corresponding author at: Yale University, New Haven, CT 06520, USA.
E-mail address: Schroers, J. (jan.schroers@yale.edu).

https://doi.org/10.1016/j.mattod.2018.07.001

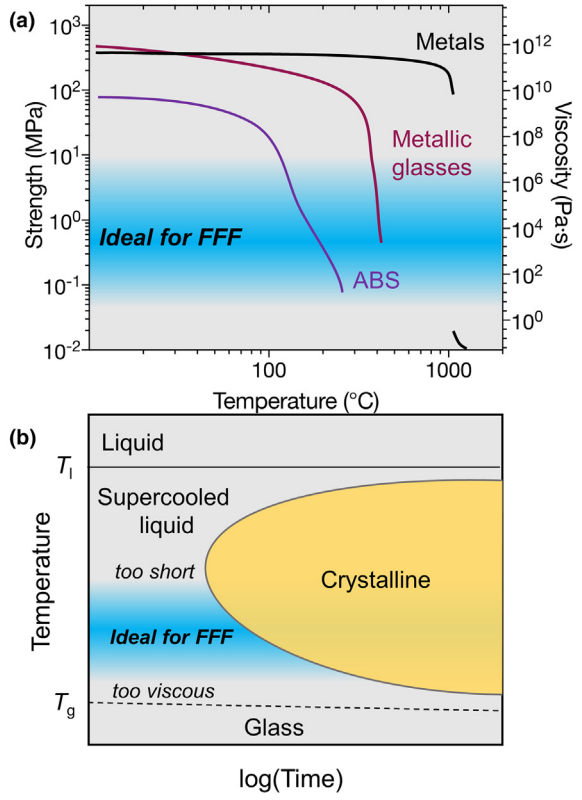

FIGURE 1

(a) Property-processability trade-off. Comparisons between material classes by their properties (strength) and their suitability for extrusion based 3D printing (such as FFF). Temperature dependent strength represents the flow stress of the material which can also be translated into a viscosity through $= \frac{\sigma}{\dot{\gamma}}$, with $\dot{\gamma} = 10^1 s^{-1}$ as a representative strain rate. The strain rate is estimated from feedstock diameter, nozzle diameter, nozzle length, and printing speed. BMGs can be processed in the ideal processing region for FFF within a viscosity range of 10^2–10^5 Pa·s, similar to typical thermoplastics like ABS (Acrylonitrile butadiene styrene). Conventional metals, on the other hand, are either by orders of magnitude too soft (in their liquid phase, bottom part of graph) or too hard (in their crystalline phase, top part of graph) for FFF processing. (b) Time-Temperature-Transformation (TTT) diagram revealing the temperature dependent time to reach crystallization. The TTT originates from the metastable nature of the supercooled liquid, which defines the available processing window for BMGs. TPF-based processing of BMGs requires a protocol balance to yield ideal behavior. This is realized through the processing temperature optimized for low viscosity yet sufficient processing time that can be experimentally realized.

[3]. The most widely used metal AM approaches are powder bed fusion processes – utilizing highly localized heating and solidification of metal powders by a laser or electron beam to locally deposit material and form a part [2,4]. While viable, these powder bed AM techniques are costly and complex to implement due to their intensive energy sources, atmosphere controls, and stringent requirements on powder size, morphology, flowability, and purity [5]. In addition, localized melting, rapid solidification, and repeated heating create complex thermomechanical stresses within as-built parts [6–8]. Such stresses often require rigid support structures to resist the accompanying deformations and complex post-processing to achieve dimensionally accurate parts [9,10]. Alternative techniques are thus being developed to realize suitable flow behavior to achieve material extrusion-based AM of metals. One strategy is semi-solid metallic extrusion, wherein extrusion is performed at a temperature such that a stable mixture of solid and liquid phases results in a suspension with a proper apparent viscosity [11,12]. Semisolid material extrusion relies on a tight control of the solid's volume fraction, and therefore of the nozzle thermal conditions. The process is robust when a large difference exists between the solidus and liquidus temperatures of the feedstock alloy, which is sufficiently wide only in a small number of alloys. Another strategy to achieve an appropriate (apparent) viscosity is to use thermoplastics as flowing and binding agents to enable FFF of metal powders [13–15]. This process essentially utilizes the available viscosity of the thermoplastics, (typical loaded metal volume fraction <60%) combined with the strength and other desirable properties of the metal (Fig. 1). The disadvantage of such processing is that it requires elaborate subsequent solvent and polymer removal followed by sintering to achieve a dense metal part. In short, the dearth of material systems which exhibit rheological behavior suitable for material extrusion is reflected in a lack of accessible metal AM technologies.

A strategy to create an accessible metal AM technology is to develop printing processes around new materials outside the traditional metals classes. A prominent example is bulk metallic glasses (BMGs) [16–18]. The amorphous structure of BMGs results in high strength and elastic limits, which is often paired with other desired properties such as high fracture toughness [19,20] and high corrosion resistance [21]. Unique among metals, BMGs relax into a (supercooled) liquid upon heating above the glass transition temperature. As in thermoplastics, this behavior can be used for thermoplastic forming (TPF) and hence permits the fabrication of metal articles with the processing methods typically associated with thermoplastic polymers, thereby escaping the property-processing trade-off [3] (Fig. 1). As the supercooled liquid is metastable, a challenge in BMG processing is to avoid crystallization through careful control of time-at-temperature (Fig. 1b). Accurate temperature control in TPF based BMG processing and carefully tailored processing temperature and time for a specific process is required [3,22].

Motivated by BMGs' superb properties and also to address their typical size limitations imposed by their maximum casting thickness, AM of BMGs have been considered in the past, however, without leveraging their thermoplastic-like processability (Fig. 1). Established laser fusion based approaches have been explored [23–27]. Limited by the same challenges as for laser fusion of crystalline metals, with an additional difficulty in avoiding crystallization, AM of fully amorphous BMGs remains challenging. For example, chemical segregation [25], microstructural heterogeneity, and partial crystallization [26,27] have been identified as major challenges for AM of BMGs.

In order to escape the property-processability trade-off, in this paper we combine both of the two above strategies, applying a new processing route (FFF-based 3D printing) to a unique material class (BMGs). We circumvent known BMG-specific challenges in additive manufacturing by taking advantage of their thermoplastic forming ability to achieve 3D printing through a FFF-based process. Under similar conditions used for thermoplastics, fully dense and fully amorphous BMG parts can be directly printed with comparable speeds and versatility as seen in FFF of thermoplastics. Some mechanical properties of the as-printed

BMG parts are comparable to the same and superb properties for as-cast BMG samples.

Materials and methods

Fabrication of BMG feedstock material

Constitutive elements of purities better than 99.9% (only considering metallic impurities) were alloyed by arc-melted in an argon atmosphere. To ensure homogenous material, sample was flipped four times. The alloyed BMG forming alloy is crystalline after this step. Subsequently, the alloy is reheated in quartz tubes under a vacuum of 10^{-3} mbar. The quartz tube has a melting section of 12 mm ID (inner diameter) and 14 mm OD (outer diameter) and a casting section of 2 mm ID and 3 mm OD. After melting for 3 min at 900 °C, the liquid BMG former is forced under argon pressure of $\sim 10^5$ Pa into the casting section where it remained for 30 s at the processing temperature of 900 °C. Subsequently, liquid BMG forming alloy, while in the casting section of the quartz tube, is water quenched, by submerging into a water container. After cooling to room temperature, a fully amorphous BMG rod is achieved.

Mechanical characterization

Tension tests were conducted with Instron 5543 under quasistatic condition with strain rate of 10^{-4} s^{-1}. The amorphous nature of metallic glasses was characterized using DSC (Perkin Elmer Diamond DSC) and XRD (Rigaku Smartlab).

Results

3D printing

$Zr_{44}Ti_{11}Cu_{10}Ni_{10}Be_{25}$ was selected as a model system to study metallic glass material extrusion because it is widely characterized, commercially available, and has high thermoplastic formability [28–30]. Amorphous $Zr_{44}Ti_{11}Cu_{10}Ni_{10}Be_{25}$ rods with 1 mm diameter and up to 70 cm length were used as printing media. These rods were fed into a heated extrusion head (Fig. 2). It was found that best results can be achieved when extruded at 460 °C, at which the time to crystallization is approximately 100 s and the viscosity is $\sim 10^5$ Pa·s [31]. At lower temperatures, the high viscosity required impractically high extrusion forces, whereas at high temperatures, accelerated crystallization kinetics required impractically short processing times (Fig. 1b). With an extrusion force range of 10–1000 N, a nozzle diameter of 0.5 mm, and an effective length in the extruder of 2 mm, $Zr_{44}Ti_{11}Cu_{10}Ni_{10}Be_{25}$ can be extruded with a rate of up to 5 cm/s. Printing was performed onto a bed of stainless steel mesh preheated to ~400 °C where the crystallization time is ~1 day [31]. The motion and extrusion system consists of a modified numerically controlled milling table, which is robotically controlled by G-code commands generated from a custom-written toolpath generation software. Motivated by our previous finding that metallurgical bonding of BMGs during TPF can be achieved by straining at the interface, even when processed in air [32], a pulsed Joule-heater was designed to locally heat the previously

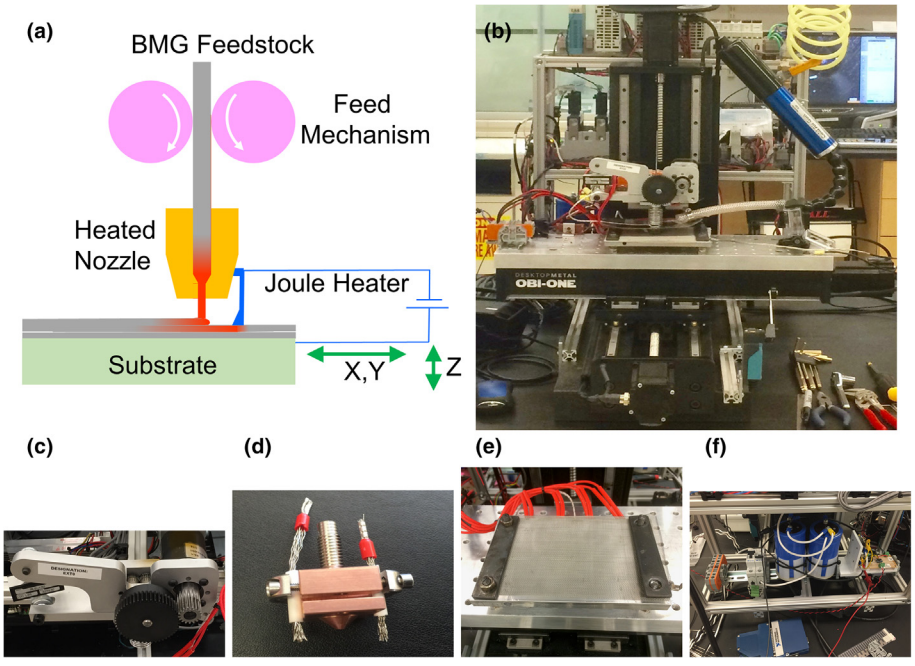

FIGURE 2

Process summary. (a) Schematics of the TPF based FFF process for direct-write extrusion of BMGs. (b) Physical setup of TPF-based BMG printer. (c) Feed mechanism which generates forces of up to 1000 N (typically <100 N are applied) to follow the G-code of maximum extrusion speeds of 5 cm/s. (d) Extrusion nozzle with Joule heater attached. The BMG feedstock is forced into the extruder head which has an effective extrusion length of 2 mm. Within the head the BMG is heated to the thermoplastic processing temperature of 460 °C to be dispensed through an orifice with an opening diameter of either 0.5 or 1 mm in diameter. Joule heating was powered by a high current voltage power supply (48 V, 72 A) that feeds into a high farad capacitor bank (1F). In order to locally heat the previous layer, a metal brush proceeds the extruder by a short distance (~1 mm). A passing pulsed-current heats predominately the contact area, and careful adjustment of current allows control of temperature to ~460 °C. (e) Heated substrate stage. Heating to 400 °C facilitates initial bonding of extruded BMG to the substrate. The substrate moves relative to the stationary extrusion head, with the two programmed by the same motion system. (f) Capacitor bank of 1F which generates for an applied voltage of 10–20 V, pulsed, 5–20 Hz currents (~10 ohms), for durations of 100–500 μs.

printed layer underneath the nozzle to a temperature similar to the extrusion temperature (Fig. 2). In order to achieve the interfacial strains required to establish a metallurgical bond between layers, the bead height (h_{bead}) and bead width (w_{bead}) were controlled such that the bead aspect ratio was in the range of $2 < \frac{w_{bead}}{h_{bead}} < 4$. Such an aspect ratio requires the extrudate to deform laterally within the printing plane, thereby establishing a strain at the interface between the current layer and the prior layer, which acts as a bonding substrate.

Using the process described in Fig. 2, a wide range of BMG parts have been printed. Printing conditions result in a volumetric build rate of ~10 mm^3/s. This build rate compares with build rates of 1–10 mm^3/s for laser powder bed fusion [26,33] and ~40 mm^3/s for thermal spray [34]. Fig. 3 shows representative printed parts in a continuous mode, where extrusion is never interrupted during printing (Fig. 3a), and in a start-stop mode, where extrusion is interrupted, e.g., at the end of each printed line (Fig. 3b). For both modes, fully dense ($\rho = 5.76$ g/cm^3) and pore-free solid BMGs can be achieved (Fig. 3c,d). During printing, the required feed force is typically <100 N but may be required to increase during start-stop to up to 1000 N. It is important to emphasize that all aspects of the printing process have been carried out in air, unique among metal 3D printing, and a tremendous benefit in the development of a practical metal 3D printing process.

Characterization of 3D printed BMG parts

Printed BMG parts have been characterized with thermal and mechanical methods (Fig. 4). To determine the effect of the printing process and the associated temperature exposure, we carried out thermal analysis (Fig. 4a) of the feedstock and printed BMGs, by differential scanning calorimetry. Thermal stability, ΔT, the temperature difference between the glass transition temperature, T_g, and the crystallization temperature, T_x, and heat of crystallization, ΔH, of the feedstock BMG are $T_g = 371$ °C, $T_x = 473$ °C, $\Delta T = 102$ °C, $\Delta H = 83 \pm 5$ J/g and of the printed BMG are $T_g = 373$ °C, $T_x = 476$ °C, $\Delta T = 103$ °C, $\Delta H = 85 \pm 5$ J/g, which are essentially identical within experimental error.

Mechanical characterization was carried out to evaluate the effect of the printing process on the mechanical properties of BMGs. Quasi-static tension was carried out on printed parts in directions both parallel and perpendicular to the printed direction (Fig. 4b). The fracture strength of the printed BMG sample, when loaded parallel to the printed layers, $\sigma_{\parallel}$, reaches up to 1220 MPa. When loaded perpendicular to the printed layers, fracture strength, $\sigma_{\perp}$, of up to 790 MPa can be achieved. For comparison, the fracture strength of the feedstock material is ~1900 MPa. $\sigma_{\perp}$ is highly sensitive to the printing conditions, particularly to the temperature difference between the extruded and the previous layer. In the extreme case, that the temperature difference between extruded BMG and previous layer is such that no deformation of the previous layer takes place, essentially no metallurgical bond forms and as a consequence $\sigma_{\perp} \sim 0$ MPa (Fig. 4c). This is due to the fact that, when processed in air, the layer to layer bonding relies on the strain of the extruded-previous layer interface to break the native oxide film on the surface, and hence, enable a metallurgical bond [32]. An interfacial strain can only be achieved if both layers, the extrudate and the previous layer, deform together. Under these conditions, their surfaces bond

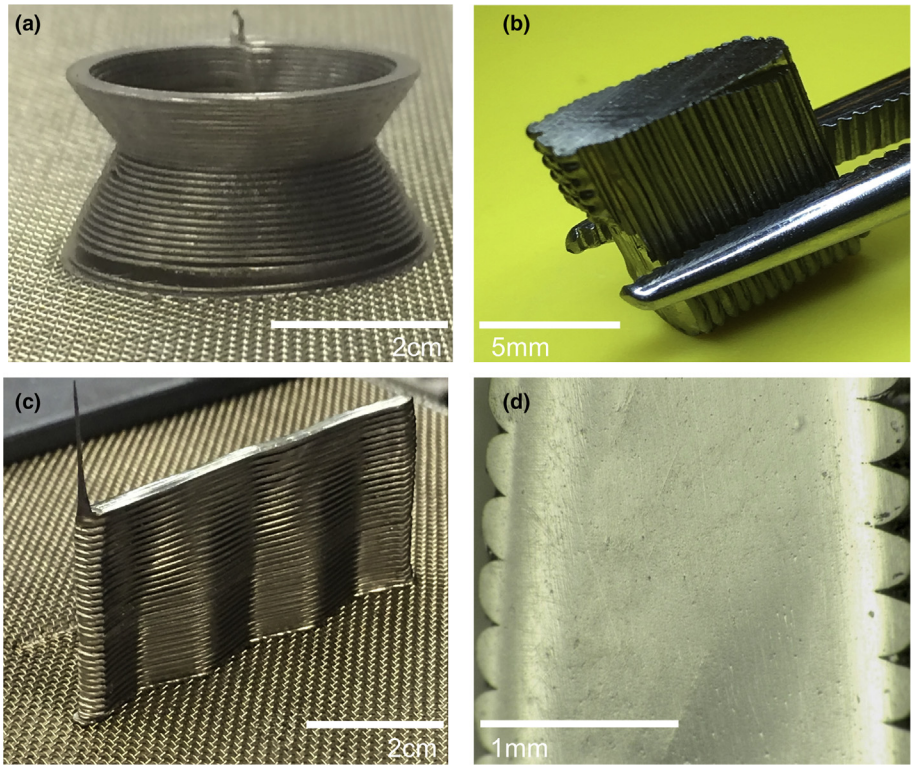

FIGURE 3

BMG parts printed via the TPF-based FFF process. (a) continuous and (b) start-stop 3D printing of the BMG extrude (scale bar length is 2 cm). (c) Fully dense and pore-free parts can be created with both modes (d) close up of (c).

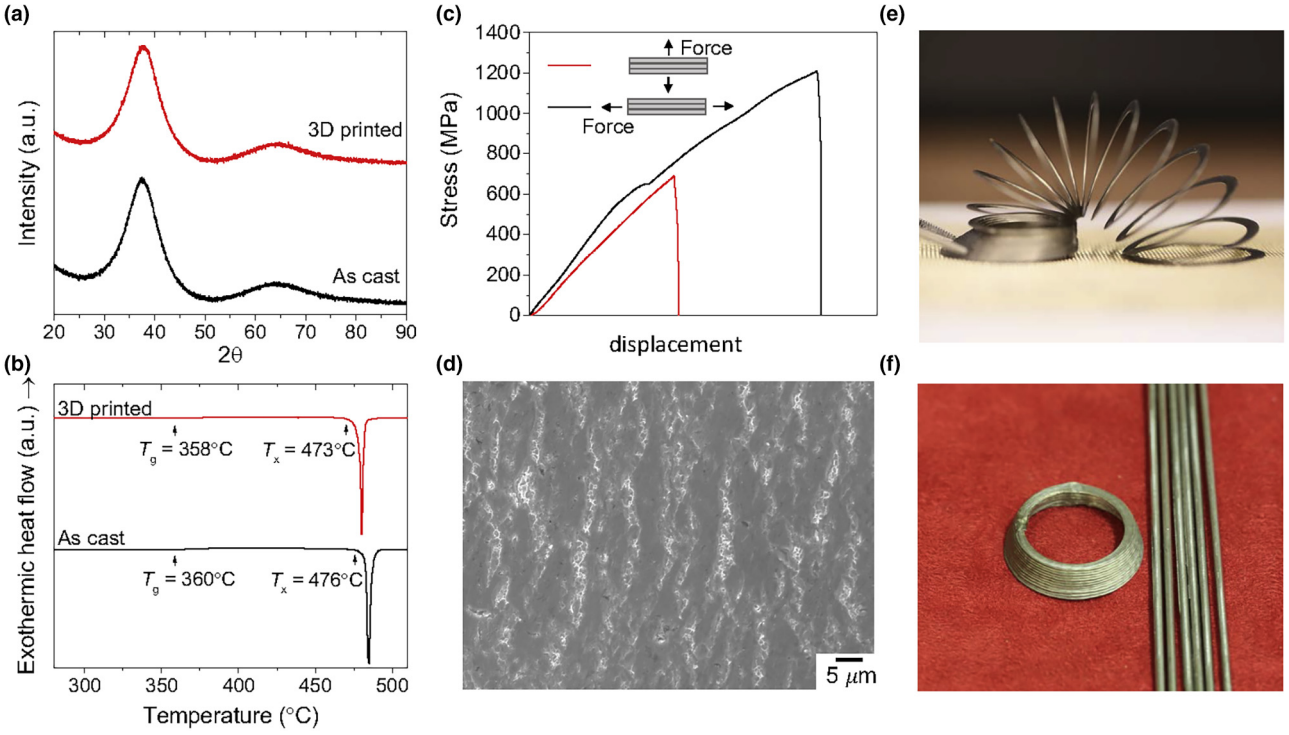

FIGURE 4

Characterization of printed BMG parts. (a) X-ray and (b) thermal analysis reveal that the TPF-based FFF of BMGs does not noticeably affect the amorphous phase. This suggests that undesirable crystallization can be avoided during 3D printing. (c) Tensile testing of 3D printed BMG parts parallel and perpendicular to the printing direction. Due to machine compliance, we do not report strain. (d) Fractured layer-layer interface. The bright vein-like regions are indicative of a metallurgical bond between the two layers and the area fraction of ~30% correlates with the achieved strength which is approximately 25% of the yield strength of the BMG. (e) Printing without Joule-heating does not lead to metallurgical bond between layers and, consequently, no significant perpendicular strength. (f) Comparison of surface appearance of BMG feedstock and 3D printed part which was printed in air. Similar appearance suggest that the low processing temperature paired with the general high corrosion resistance of BMG suggest that printing can be readily carried out in air and does not require elaborate vacuum or inert gas conditions which are required for all other metal 3D printing methods.

rather than re-oxidize. Hence, the temperature of the previous layer at the location where the extruded material makes contact must be similar to the extruded temperature. For the printed BMGs with $\sigma_{\perp}$ = 790 MPa, where a similar temperature between extruded and previous layer was established, the fractured surface shows regions where a metallurgical bond has occurred (Fig. 4e). The area fraction of the metallurgically bonded regions, which occur bright and vein-like in Fig. 4e, of ~30% is comparable to the ratio of inter-layer bond strength of the 3D printed material to bulk strength, 790 MPa/1900 MPa, confirming the thermoplastic strain bonding mechanism [32].

Unique among metal 3D printing processes, and a major advantage of the introduced 3D printing of BMGs through FFF method is that the entire process can be carried out in air. Thermal and mechanical behavior (Fig. 4a,b,c,e) suggest no noticeable effect of the air exposure during fabrication. Further, when considering the temperature exposure during the printing process (Fig. 4f) no discoloration, which would be indicative of oxidation, can be discerned. This is initially surprising, as $Zr_{44}Ti_{11}Cu_{10}Ni_{10}Be_{25}$ BMG comprises reactive elements. However, when combined in the amorphous phase they appear more robust against oxidation, which, together with the low processing temperature for TPF-based processing, permits processing in air [3,35].

Discussion

Most of presented research has been focused on $Zr_{44}Ti_{11}Cu_{10}Ni_{10}Be_{25}$ BMG, that we chose due to its practicality. Further, printing speed, nozzle diameter, and printing forces have not yet been varied systematically to map out processing parameter space. To extend the discussion to a broader range of processing parameters and BMG compositions, we consider the flow of a viscous liquid through the extrusion nozzle (Fig. 5). The extrusion process in the FFF process using TPF of BMGs can be essentially regarded as an extrusion flow process of a high-viscosity Newtonian fluid [36] through a heated cylindrical die. The overall high viscosities of the flowing BMG material results in Reynolds numbers close to zero, i.e., creeping flow conditions [36]. Therefore, the required extrusion pressure, P, can be approximated by:

$$P = \frac{32\eta L v}{d^2} \quad (1)$$

where η is the viscosity of the BMG, L is the effective die length, v is the extrusion rate, and d is the diameter of the orifice. Eq. (1) allows us to estimate the required forming force to establish a target printing speed for various orifice diameters (0.5, 1, and 2 mm) as a function of the viscosity. For Fig. 5, we assumed an orifice length of L = 2 mm and a target extrusion speed of 5 cm/s, which

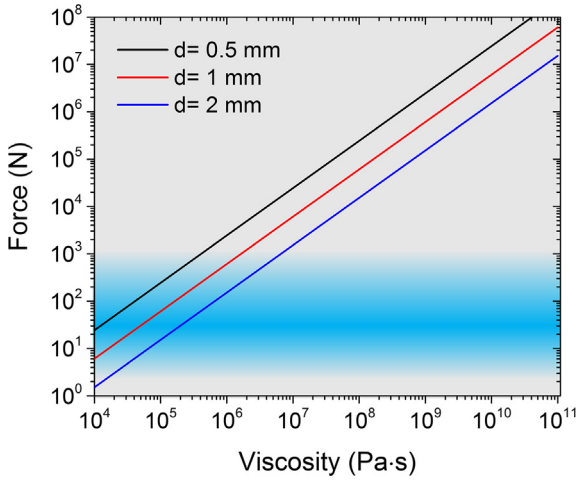

FIGURE 5

Calculations of extrude-ability of BMGs depending on their viscosity and crystallization time characteristics. A preferred extrusion force would be in the 10–1000 N range (indicated by the blue region) where precise control is possible and forces are sufficiently small that they can be realized in practical printers. For the short (peak) temperature exposure during printing of 0.1 −1s, viscosities of 10^4–10^5 Pa·s can be realized in highly formable BMGs such as the considered $Zr_{44}Ti_{11}Cu_{10}Ni_{10}Be_{25}$, 10^6–10^7 Pa·s for BMGs with medium formability such as ZrNiCuAl alloys, and 10^7–10^8 Pa·s for the less formable BMGs such as Fe-based BMGs. This suggests that highly formable BMGs can be readily printed even with 0.5 mm diameter nozzles, medium range BMGs with 0.5–1 mm nozzles, and the less formable BMGs only with 2 mm nozzles.

are similar to our experimental conditions. We showed previously that entry effects are small for the here considered orifice length and diameter [36]. For practical reasons a printing force of 10–1000 N is desirable; printing forces exceeding 1000 N are difficult and expensive to realize in 3D printers whereas forces below 10 N become increasingly difficult to control. Such ideal printing behavior can be realized for BMGs with viscosities below 10^6 Pa·s when printing through a 0.5-mm orifice, and below 10^8 Pa·s when printing through a 2-mm orifice. For a BMG to qualify for such a process, the available time before crystallization must exceed the time the BMG is exposed to corresponding temperature during the FFF process. As the time exposure during the extrusion process can be readily reduced below one second, viscosities of 10^4–10^5 Pa·s can be realized in highly formable BMGs such as the considered $Zr_{44}Ti_{11}Cu_{10}Ni_{10}Be_{25}$ [22], viscosity values of 10^6–10^7 Pa·s for BMGs with medium formability such as ZrNiCuAl alloys, and 10^8–10^9 Pa·s for the less formable BMGs such as Fe-based BMGs. This suggests that highly formable BMGs can be readily printed under practical conditions even with 0.5-mm diameter nozzles, whereas medium range formable BMGs with 0.5–1-mm nozzles, and the less formable BMGs only with 2-mm nozzles.

Conclusions

The present BMG 3D printing process offers a solution to escape the property-processability tradeoff. Processability has been realized by utilizing the gradual softening of thermoplastically formable BMGs for a direct extrusion process, paired with an interlayer metallurgical bonding mechanism. For properties, quasistatic tensile strength is the highest reported value for AM BMG parts and among the highest for any AM metal part [33,37,38].

The ability to carry out this process in air is of practical importance as it avoids costly and typically complicated inert or vacuum conditions. The low TPF processing temperatures during printing and the absence of a first-order phase transition of the BMG during solidification after extrusion results in little shrinkage, at least one order of magnitude less than the shrinkage of liquid-based additive manufacturing processes for conventional metals [2].

A comparison to widely established FFF of thermoplastics, a mature and commercially available technology, suggests a high degree of similarity. It is therefore plausible that many of the engineering challenges that have been solved in thermoplastic FFF can be readily translated to the printing of BMGs. As a consequence, we look forward to a period of potentially rapid progress in 3D printing of BMGs.

Acknowledgments

The characterization of the printed parts was funded under ONR's "Additive Manufacturing of Alloys for Naval Environments" program.

Appendix A. Supplementary data

Supplementary data associated with this article can be found, in the online version, at https://doi.org/10.1016/j.mattod.2018.07.001.

References

[1] M.F. Ashby, Acta Metall. Mater. 39 (6) (1991) 1025.
[2] D. Herzog et al., Acta Mater. 117 (2016) 371.
[3] J. Schroers et al., Mater. Today 14 (1–2) (2011) 14.
[4] Y.M. Wang et al., Nat. Mater. 17 (1) (2018) 63.
[5] T. DebRoy et al., Prog. Mater. Sci. (2017).
[6] P. Mercelis, J.P. Kruth, Rapid Prototyp. J. 12 (5) (2006) 254.
[7] A.S. Wu et al., Metall. Mater. Trans. A 45a (13) (2014) 6260.
[8] A. Dunbar et al., Addit. Manuf. 12 (2016) 25.
[9] K. Zeng et al., Addit. Manuf. 6 (2015) 67.
[10] W.E. King et al., Appl. Phys. Rev. 2 (2015) 4.
[11] C.S. Rice et al., Jom-J. Minerals Metals Mater. Soc. 52 (12) (2000) 31.
[12] W. Chen et al., Appl. Phys. Lett. 110 (9) (2017). 094,104.
[13] M.K. Agarwala et al., Sol. Freeform Fabric (1996) 385.
[14] S.L. Taylor et al., Acta Mater. 143 (2018) 20.
[15] A.E. Jakus et al., Adv. Funct. Mater. 25 (45) (2015) 6985.
[16] A.L. Greer, Science 267 (5206) (1995) 1947.
[17] W.L. Johnson, MRS Bull. 24 (10) (1999) 42.
[18] J. Schroers, Phys. Today 66 (2) (2013) 32.
[19] M.F. Ashby, A.L. Greer, Scripta Mater. 54 (3) (2006) 321.
[20] J.J. Lewandowski et al., Phil. Mag. Lett. 85 (2) (2005) 77.
[21] S.J. Pang et al., Acta Mater. 50 (3) (2002) 489.
[22] W.L. Johnson et al., Science 332 (6031) (2011) 828.
[23] S. Pauly et al., Mater. Today 16 (1–2) (2013) 37.
[24] Y.Q. Li et al., J. Mater. Process. Tech. 248 (2017) 249.
[25] X. Li et al., Mater. Sci. Eng. A 606 (2014) 370.
[26] D. Ouyang et al., Intermetallics 90 (2017) 128.
[27] Y. Shen et al., J. Non-Cryst. Solids (2017).
[28] W. Chen et al., Scripta Mater. 107 (2015) 1.
[29] Z. Liu et al., Acta Mater. 105 (2016) 35.
[30] J. Schroers, Acta Mater. 56 (3) (2008) 471.
[31] T. Waniuk et al., Phys. Rev. B 67 (2003) 18.
[32] W. Chen et al., Acta Mater. 62 (2014) 49.
[33] P. Bordeenithikasem et al., Addit. Manuf. (2018) 95.
[34] C. Zhang et al., J. Mater. Chem. A 6 (16) (2018) 6800.
[35] U. Koster, L. Jastrow, Mat. Sci. Eng. A-Struct. 449 (2007) 57.
[36] H.M. Chiu et al., Scripta Mater. 61 (1) (2009) 28.
[37] J.J. Lewandowski, M. Seifi, Ann. Rev. Mater. Res. 46 (2016) 151.
[38] X.Y. Zheng et al., Science 344 (6190) (2014) 1373.